

# Cognition of Parameters' Role on Vertical Control Device for Aerodynamic Characteristics of Aircraft Using Data Mining

Kazuhisa Chiba<sup>1</sup> \*; Taiga Omori<sup>2</sup>, Yasuto Sunada<sup>2</sup>, and Taro Imamura<sup>2</sup>

<sup>1</sup> Graduate School of Informatics and Engineering,  
The University of Electro-Communications,  
1-5-1, Chofugaoka, Chofu, Tokyo 182-8585, Japan

<sup>2</sup> Department of Aeronautics and Astronautics,  
The University of Tokyo,  
7-3-1, Hongo, Bunkyo, Tokyo 113-8656, Japan

April 14, 2015

## Abstract

The new concept to place the vertical airfoil device as control surface has been discovered so as to improve the aerodynamic performance of aircraft. The concept was predicated on not only the several devices as vortex generator and winglet but also the wing-mounted engine system of the HondaJet. Thereupon, the wind tunnel experiment has been implemented in order to investigate the influence of the vertical control device with the symmetrical airfoil shape. Furthermore, a self-organizing map as data mining has been performed for the experimental data in order to qualitatively elucidate the correlations among the aerodynamic performances as design requirements and the design parameters to place the vertical control device. Consequently, it has been revealed the design information regarding the intimate correlations. Moreover, there is the sweet spot in the design space to improve the aerodynamic performances.

Keyword: Vertical device; Control surface; Aerodynamics of aircraft;  
Data mining; Self-organizing map.

---

\*kazchiba@uec.ac.jp

# 1 Introduction

Although the surface of the main wing of aircraft, especially upper wing surface, is generally desirable to be smooth in ordinary design of an aircraft, there are several exceptions to this universal tacit knowledge[6, 9], such as small devices for flow control. Honda Aircraft Company has designed and developed a business jet aircraft named as the HondaJet[3]. Despite the fact that the devices are generally designed small on general knowledge even when devices will be on the wing surface, the HondaJet mounts its engine over the upper surface of the wing with the pylon. The design of the HondaJet astonishingly reveals that the optimum location of the nacelle and the cross section of the pylon exists to accomplish lower drag coefficient compared with the clean wing[4]. This fact indicates that the devices on the wing surface, whose size is independent on the convention of aircraft design, can uncommonly improve the aerodynamic performance of aircraft.

Thereupon, in the present study, a new basic idea regarding a vertical control device on the upper surface of the main wing will be proposed in order to improve the aerodynamic performance of aircraft due to the flow control on the wing surface. The devices are expected to be also installed on the trailing edge of the pylon in order to improve the aerodynamic performance. Therefore, the objective of the present study is to elucidate the effectiveness on the aerodynamic performance regarding the control surface which is vertically mounted on the wing. As a first step, the wind tunnel experiment is implemented in order to quantitatively reveal its effectiveness[7]. As a second step, data mining is performed by using a self-organizing map for the experimental data so that the global design information for the design space will be also efficiently revealed. Especially, the keystone of the present treatise corresponds to the second step. The objectives of the present data mining are that significant experimental conditions are efficiently addressed from  $10^3$ -order conditions. Furthermore, the obtained design knowledge will be utilized in order to generate a wind tunnel model for the next-step experiments so that a vertical control device is efficiently installed and its optimum geometry will be designed.

# 2 Problem definition

The simple symmetrical aircraft model constructed by the main and tail wings with rectangular planform and vertical control device is developed in order to utilize in the wind tunnel experiment. The specification of an

Table 1: Specification of aircraft model for wind tunnel experiment.

<i>component</i>	<i>content</i>	<i>data</i>
fuselage	length	370 [mm]
	width	44 [mm]
	height	55 [mm]
main wing	span length	404 [mm]
	chord length	80 [mm]
	airfoil	NACA2410
	aspect ratio; $AR$	5.05 [-]
	taper ratio	1.0 [-]
vertical control device	chord length	40 [mm]
	span height	40 [mm]
	airfoil	NACA0010

Table 2: Design parameters and their discretized design space.

<i>description</i>	<i>symbol</i>	<i>design space</i>
spanwise distance	$\mu$ [mm]	$10 \leq \mu \leq 170$ for every 10
deflection angle	$\delta$ [deg]	$-10 \leq \delta \leq 10$ for every 2
angle of attack of body	$\alpha$ [deg]	$-6 \leq \alpha \leq 20$ for every 2

aircraft model is shown in Table 1. The fuselage and tail wings constructed by the plane surfaces are fixed. The main wing itself is fixed, however, the vertical control device is shifted on the upper surface of the main wing[7]. Thereupon, the model geometry is defined by the following three design parameters. The first is the spanwise distance from the root of the main wing to the installed position of the vertical control device  $\mu$  [mm]. The second is the deflection angle of the vertical control device onto the upper surface of the main wing  $\delta$  [deg]. The illustrated description of these two design parameters is shown in Fig. 1. The third is the angle of attack of the body  $\alpha$  [deg]. The design space of the each design parameter is summarized in Table 2. Since the experiment cannot strictly set the values of the design parameters, the three design parameters have not continuous but discretized values.  $\mu$  is the distance between the root of the main wing (that is, body wall) and the 25% position of the mean aerodynamic chord for the vertical control device.  $\mu$  moves from 10 to 170 [mm] for every 10 [mm]. The two vertical control devices are symmetrically set on the main wing.  $\delta$  is the deflection angle of the vertical control device onto the main wing. The revolutionary center is set on the 25% mean aerodynamic chord of the vertical control device.  $\delta$  is

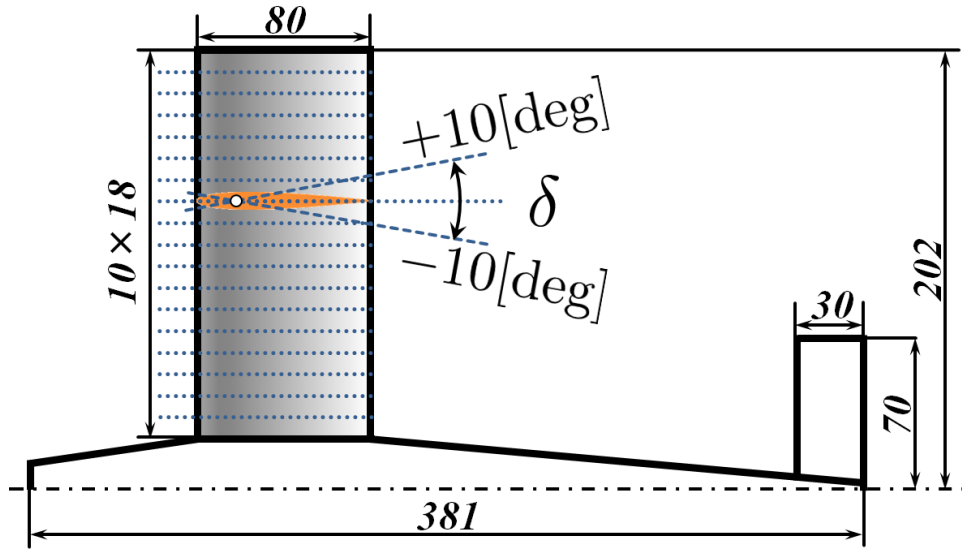


Figure 1: Bird's-eye illustration of overall geometry. The dotted lines on the main wing describe the 17 installation positions (the length from the body wall denotes  $\mu$ ) of the vertical control device colored by orange. The 25% position of the mean aerodynamic chord for the vertical control device is described by the white point in the orange color.

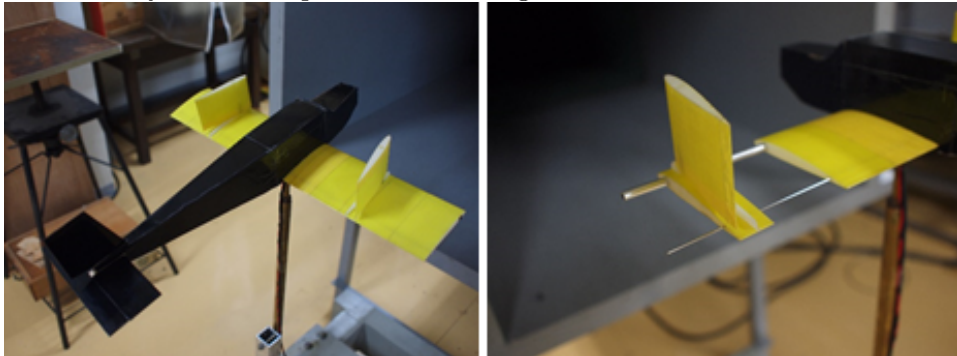


Figure 2: The wind tunnel model constructed by the separated wing blocks.

defined to be the positive value when the trailing edge of the vertical control device is installed on the outboard side shown in Fig. 1.  $\delta$  changes from  $-10$  to  $+10$  [deg] for every 2 [deg]. Note that there are no experimental data in the case of  $\mu$  of 10 [mm] and  $\delta$  of  $-10$  [deg] because the vertical control device interferes in the fuselage.  $\alpha$  changes from  $-6$  to  $+20$  [deg] for every 2 [deg].

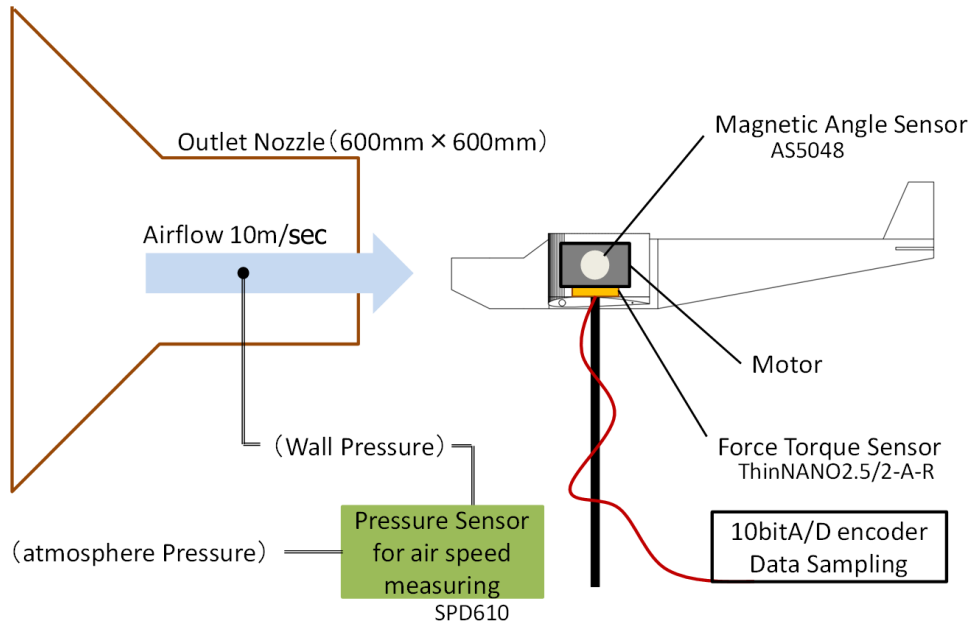


Figure 3: Schematic illustration of the system for the wind tunnel experiment.

The total number of experimental conditions is 2,604. Geometry is designed by using a computer-aided design software and it is outputted as the stereo lithography data to generate the wind tunnel model.

The wind tunnel model is made from wood. It is constructed by several elements in order to simply alter the geometry for all conditions of the wind tunnel experiments. The appearance of the wind tunnel model and the elements of the main wing are shown in Fig. 2.  $\mu$  can be moved by inserting blocks in the different order along the spar. Each wing block is made by using 3-dimensional printer. The vertical control device is also separately constructed and it is attached onto the main wing with a screw so that  $\delta$  can be simply changed. There are gaps between the leading and trailing edges of the vertical control device and the upper surface of the main wing, however, they are negligible small.

### 3 Experimental result

The experiment was performed by using the blow-down wind tunnel at the department of aeronautics and astronautics, the University of Tokyo. Its

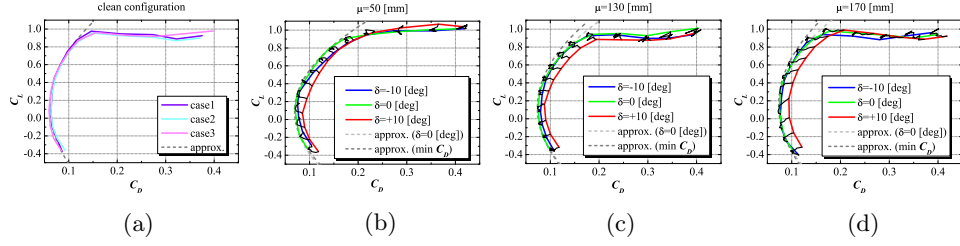


Figure 4: Polar curves. (a) clean configuration, (b) installed configuration at  $\mu = 50$  [mm], (c) installed configuration at  $\mu = 130$  [mm], and (d) installed configuration at  $\mu = 170$  [mm],

outward form has 600 [mm] height and width. The flow velocity was set to be 10 [m/sec] for all experimental conditions. The Reynolds number based on the chord length as the reference one was approximately  $5.0 \times 10^4$ . All of the experiments were carried out for 10 [sec] with the sampling frequency of 1,000 [Hz]. Therefore, all of the data regarding the aerodynamic performance obtained from the experiments are the time-averaged value of 10,000 points for 10 [sec]. Figure 3 shows the conceptual illustration of the present measurement system for the present wind tunnel experiment.  $\alpha$  was controlled by the microcomputer using a proportional-integral-derivative controller. Three aerodynamic performances of the body as a whole, the lift  $L$ , the drag  $D$ , and the pitching moment  $M_p$ , are gauged by using the wind tunnel balance. These performances are respectively transformed into the lift coefficient  $C_L$ , the drag coefficient  $C_D$ , and the pitching moment coefficient  $C_{Mp}$ , which describe the following equation divided by the dynamic pressure using the air density  $\rho$ , the velocity  $v$ , and the planform area of the main wing  $S$  as the reference one.

$$C_{\square} = \frac{\square}{\frac{1}{2}\rho v^2 \cdot S}, \quad (1)$$

where,  $\square$  denotes  $L$ ,  $D$ , and  $M_p$ .

The Oswald efficiency factor  $e$  is selected as an indicator to preliminary evaluate the aerodynamic performance of the aircraft[8]. The factor  $e$  is calculated by using the following equation.

$$e = \frac{1}{K} \cdot \frac{1}{\pi AR}, \quad (2)$$

where, the drag-due-to-lift factor  $K$  is defined as a leading coefficient of the quadratic approximation function due to  $C_L$  under the consideration of  $C_D$

as function of  $C_L$ .

$$C_D = C_{D_0} + K \cdot (C_L - C_{L_0})^2. \quad (3)$$

$C_{D_0}$  denotes  $C_D$  caused by the other drag mechanisms.  $C_{L_0}$  is physically caused by the vertical asymmetry such as a cambered wing and a finite angle of incidence. When the lift of a wing is elliptically distributed along the span,  $K$  is defined to be 1.  $AR$  denotes the aspect ratio of the main wing, whose value is summarized in Table 1.

Figure 4 shows the polar curves under the several conditions. Figure 4(a) shows the repeatability of the polar curve for the clean configuration implemented three times on different days. Since the three lines precisely correspond each other, the reproducibility of the present experiment can be elucidated. When the  $K$  is calculated by using eq. (3) for the average of three data shown in Fig. 4(a), the wind tunnel model without the vertical control device found to be  $e = 0.6505$ . Note that the correlation between the dotted line and the other three lines in Fig. 4 shows the accuracy of  $K$ . Figure 4(a) shows that the curve generated by the quadratic approximation function exactly describes the polar curves by the experiment.

Figures 4(b), (c), and (d) respectively show the polar curves by changing  $\delta$  from  $-10$  to  $+10$  [deg] under the conditions of  $\mu$  of 50 [mm], 130 [mm], and 170 [mm]. The dotted curve is quadratic approximation as eq. (2) with the points of  $-4 \leq \alpha \leq 12$  [deg]. Figure 4 reveals that the shape of polar curve becomes similar to that for the clean configuration as  $\mu$  is larger. The curvature of polar curve becomes larger as  $\mu$  is smaller. Although  $C_D$  is moved to right direction due to  $C_D$  by the vertical control device, the geometry of the polar curve is similar in the case of  $\mu$  of 170 [mm]. Although  $C_D$  at  $\delta = 0$  is found to be low around low angle of attack, there are  $\delta$  that gives larger  $C_L/C_D$  than that of  $\delta = 0$ , when  $\alpha$  is higher than 6 [deg]. When optimum  $\delta$  is selected according to the angle of attack, the data is on the envelope curve and  $e$  will be improved. The results based on this procedure are summarized in Table 3. In both cases of  $\mu = 130$  and 170 [mm],  $e$  is improved. Especially, it is almost the identical as the clean configuration for the case of  $\mu = 170$  [mm].

On the other hand, in the cases of  $\mu = 50$  and 90 [mm], there is not as much improvement as cases of  $\mu = 130$  and 170 [mm]. In Fig. 4(d), the case of  $\delta = 0$  gives the best  $C_L/C_D$  except the cases of high angle of attack. In Fig. 5, there is considerably the interference between  $\delta$  and  $C_{Mp}$ , and also between  $\delta$  and  $C_L$ . When  $\delta$  is positive value,  $C_L$  tends to be lower and  $C_{Mp}$  tends to be higher. In contrast, the negative  $\delta$  oppositely affects on  $C_L$  and  $C_{Mp}$ . The reason of these effects is that the vortex generated

Table 3: Comparison of  $e$  for several experimental conditions.

$\mu$ [mm]	max $e$ [-]	
	$\delta = 0$ (fixed)	$\delta$ (variable)
clean	0.6505	
50	0.4531	0.4273
90	0.4535	0.4718
130	0.4875	0.5633
170	0.5471	0.6513

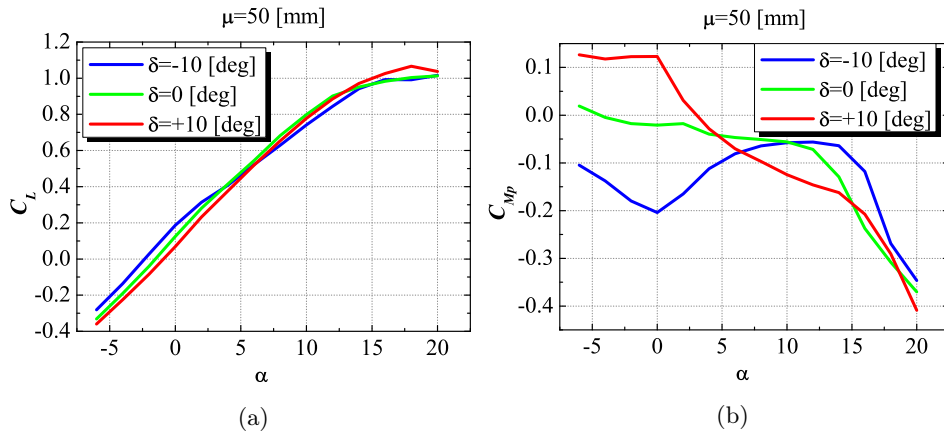


Figure 5: Comparison of the aerodynamic performance of the installed configuration at  $\mu = 50$  [mm]. (a)  $C_L$ - $\alpha$  and (b)  $C_{Mp}$ - $\alpha$ .

from the tip of the vertical control device passes in the vicinity of the tail wings, when  $\mu$  is small value such as  $\mu = 50$  [mm]. Changing the value of  $\delta$  from positive to negative reverses the rotational direction of the tip vortex by the vertical control device so that the interference for  $C_L$  and  $C_{Mp}$  is also opposite. There was little improvement on  $e$  under the condition of  $\mu = 50$  [mm] configuration because the positive effect of  $\delta \geq 0$  and negative effect of the tip vortex on the vertical control device shown in Fig. 5(a) cancelled each other.

## 4 Data-mining technique

In the present study, a self-organizing map (SOM)[5] is selected as a data-mining technique because the primary objective of data mining is the ac-

quisition of global design information in order to implement the structuring of design space. The previous study[1] indicated that SOM extracted the global design information for whole design space. The distinguishing feature of SOM is the generation of a qualitative description. The advantage of this method contains the intuitive visualization of two-dimensional colored maps of design space using bird's-eye-views. As a result, SOM reveals the tradeoffs among objective functions. Moreover, SOM addresses the effective design parameters and also reveals how a specific design parameter gives effects on objective functions and other design characteristics. One SOM is colored for one variable of objective function, design parameter, and other characteristic value so that the coloration pattern is compared with each other. Therefore, data mining using SOM might have a disadvantage to overlook important correlation in the problem with a large number of objective functions and design parameters. Since the present study has a total number of 9 at most among the design requirements, design parameters, and other variables that the influence will be observed, SOM is sufficient for the data mining manner.

In the present study, SOMs are generated by using commercial software Viscovery<sup>®</sup> SOMine 4.0 plus produced by Eudaptics, GmbH[2]. The uniqueness of the map generated by SOMine is assured due to Kohonen's Batch SOM algorithm and search of the best-matching unit for all input data and

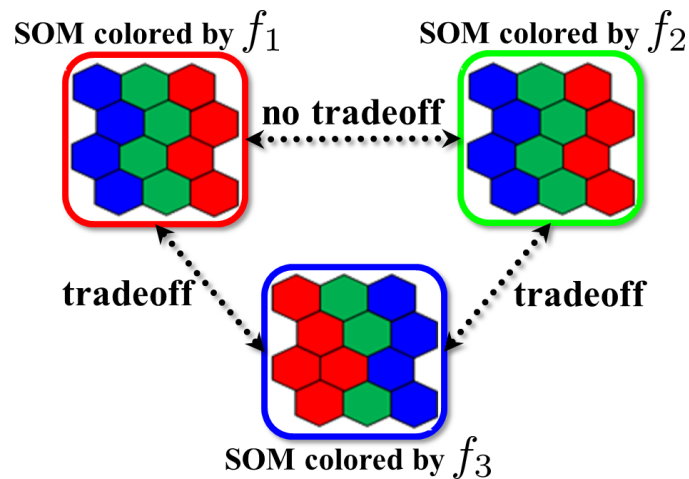


Figure 6: Comparison example of colored SOMs for minimization problem with three objective functions as  $f_1$ ,  $f_2$ , and  $f_3$ . Red describes high value and blue is low one.

the adjustment of weight vector near the best-matching unit. The decoding manner of SOM is briefly explained by using Fig. 6. This figure is assumed to be SOMs colored by three objective functions on the minimization problem of three objective functions. The generated SOM is made from hexagonal grid, which has the values of objective functions and design parameters as a vector quantity. Grids are distributed on a two-dimensional rectangular surface by the affinity of each objective-function value. Thereupon, grids with high affinity of each objective-function value clusters around a grid. There is no physical import on the vertical and horizontal lines of SOM. The comparison among SOMs to be colored by each vector quantity in each grid intuitively reveals the correlations among each vector quantity. There is similar coloration pattern between SOMs for  $f_1$  and  $f_2$  shown in Fig. 6. This comparison shows that one objective function absolutely has a low value, when another objective function has low value. Moreover, one objective function absolutely has high value, when another objective function has high value. That is, this comparison indicates that there is no tradeoff between  $f_1$  and  $f_2$ . On the other hand,  $f_3$  absolutely becomes large, when  $f_1$  becomes small, and vice versa. This comparison proves to be a severe tradeoff between  $f_1$  and  $f_3$ .

## 5 Data-mining result

The coloration pattern of SOM depends on indicator. Multiobjective optimization problems generally use objective functions as the indicator to generate SOM. However, both of the design requirements, i.e.,  $C_L$ ,  $C_D$ , and  $C_{Mp}$  and the design parameters have a major role in the present problem. Thereupon, as the first step, the SOM which the design requirements take charge of the indicator will be observed. As the second step, the SOM which the design parameters take charge of the indicator will be observed in this chapter. The especial design parameters to improve the aerodynamic performances will be specified so as to address the experimental condition and to efficiently reveal the flow mechanism.

### 5.1 Case to generate using design requirements

Figure 7 shows the SOM generated by the values of the three design requirements. As this SOM learning is implicated based on the values of the design requirements as the indicator for the similarity on the neural network, the SOMs colored by the design requirements have absolutely gradation shown in Fig. 7(a). The SOM colored by design requirement can generally indicate

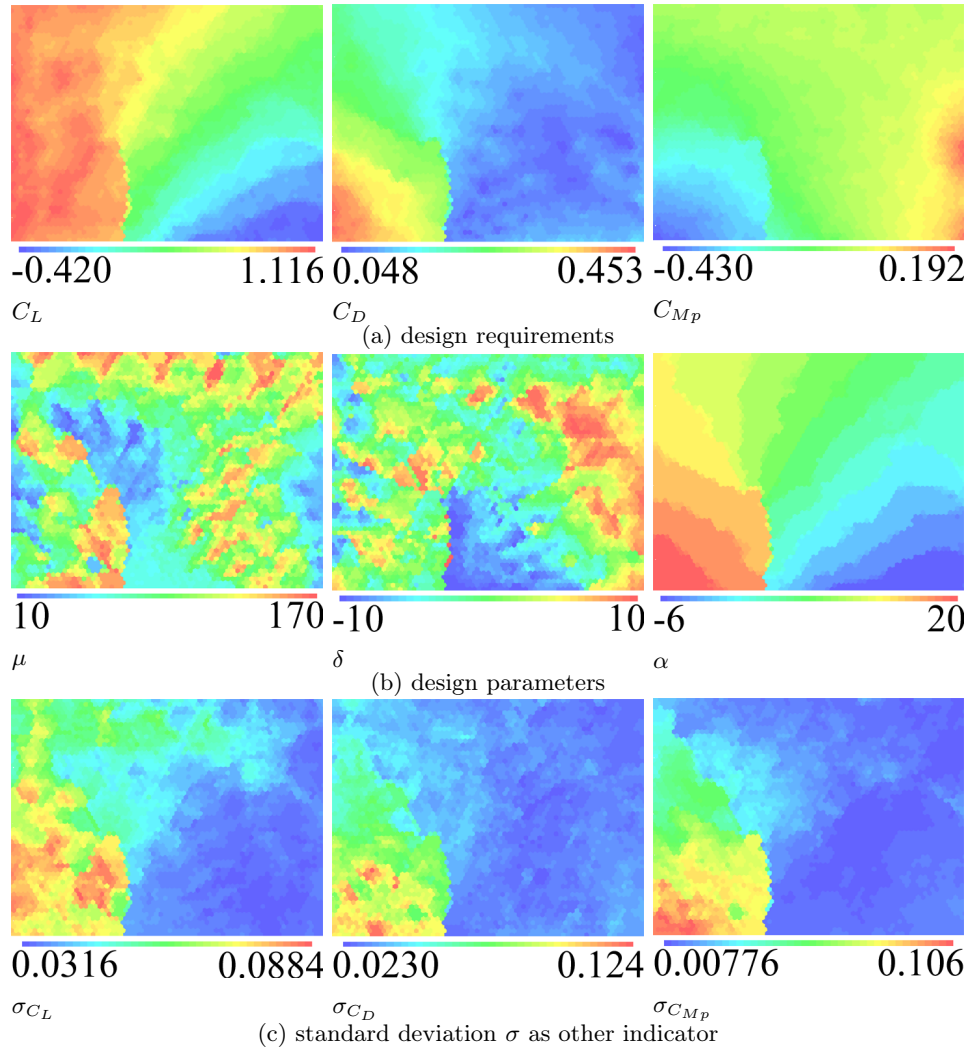


Figure 7: SOM generated by design-requirements values.

not only tradeoff information but also optimum and pessimum direction on SOM due to the gradation. In addition, the directions of the influence of design parameters for design requirements can be observed by comparison between the SOMs colored by the design requirements and those by the design parameters.

The SOMs colored by  $C_L$  and  $C_D$  in Fig. 7(a) reveal that there is a tradeoff between them. However, coloration patterns of  $C_L$  and  $C_D$  for

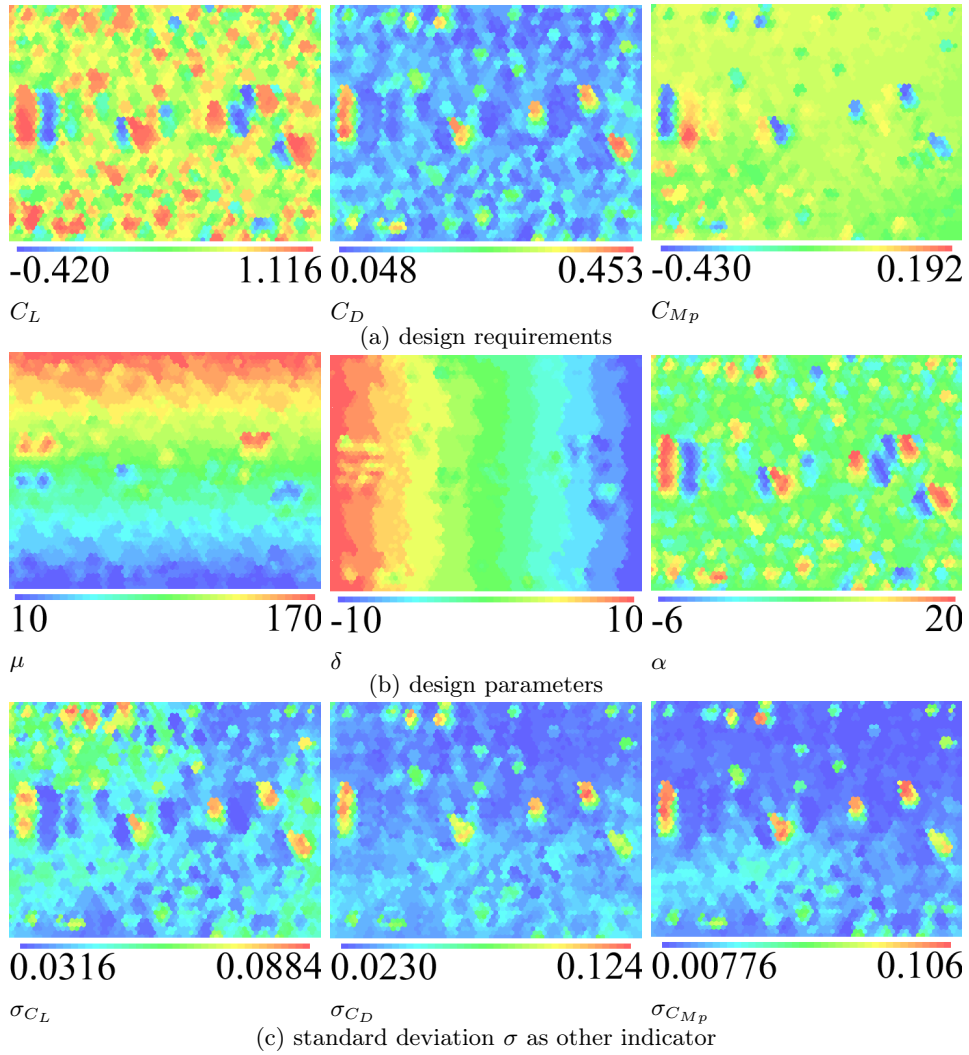


Figure 8: SOM generated by design-parameters values.

both the maximum and minimum directions are different. The compromise design region can be relatively found out on the SOM. The SOM colored by  $C_{Mp}$  in Fig. 7(a) reveals that the SOM's region to be the low value of  $C_{Mp}$  corresponds to that to be the high value of  $C_D$ . On the other hand, although the SOM's region to be the high value of  $C_{Mp}$  exists the bottom right on the SOM, the coloration pattern of it is unique. Note that  $C_{Mp}$  should be generally zero for the trim of the aircraft. The trim is practically gained by

controlling the elevators. Since the elevators of the present body are fixed, the present  $C_{Mp}$  cannot indicate the optimum and pessimum directions. Correlations between  $C_{Mp}$  and the other two aerodynamic characteristics as  $C_L$  and  $C_D$  are merely observed.

The SOMs colored by the three design parameters as  $\mu$  [mm],  $\delta$  [deg], and  $\alpha$  [deg] are shown in Fig. 7(b). The SOM colored by  $\mu$  reveals that  $\mu$  does not have direct influence on the three design requirements. Although there is a possibility that the combination between  $\mu$  and  $\delta$  gives the effects on the design requirements, Figs. 7(a) and (b) does not indicate it. The SOM colored by  $\delta$  reveals that the low value of  $\delta$  gives an effect on the low value of  $C_D$ . The high value of  $\delta$  does not directly give effects on the three design requirements. The SOM colored by  $\alpha$  reveals that the high value of  $\alpha$  directly affects on the high value of  $C_D$  and also the low value of  $\alpha$  directly gives an effect on the low value of  $C_L$ . Since  $\alpha$  generally has the effects on the aerodynamic performance, these results make sense. Since the coloration pattern shown in Figs. 7(a) and (b) depends on  $\alpha$ ,  $\alpha$  should be omitted so that the influences of  $\mu$  and  $\delta$  are observed.

Figure 7(c) shows the SOMs colored by the standard deviation  $\sigma$  for the three design requirements as  $C_L$ ,  $C_D$ , and  $C_{Mp}$ . The present  $\sigma$  is defined as the standard deviation for the data of 10,000 points for 10 [sec] in an experimental condition. These figures reveal that these have similar coloration pattern, and  $\sigma$  has high value when  $\alpha$  becomes high. This fact suggests that  $\sigma$  increases after the stall. The SOM generated by the three design parameters as  $\mu$ ,  $\delta$ , and  $\alpha$  is prepared in Fig. 8 in order to directly observe the influence of them on the three design requirements. The coloration patterns of  $C_L$  and  $C_D$  reveal that there is no regularity for those of  $\mu$  and  $\delta$ . That is, the coloration patterns of the design requirements indicate that the design requirements strictly depend on  $\alpha$ . Thereupon, the influence of  $\alpha$  on the three design requirements should be erased in order to directly observe the influence of  $\mu$  and  $\delta$ .

## 5.2 Case to generate using two design parameters as $\mu$ and $\delta$

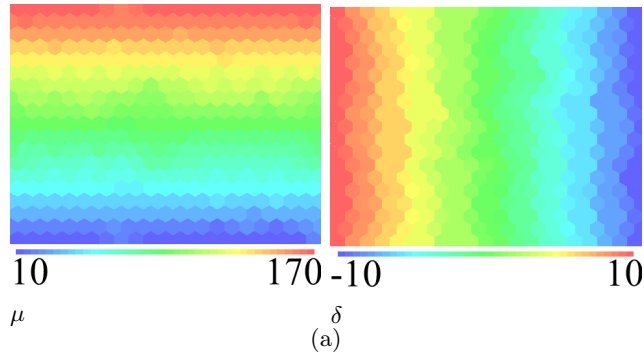
The SOM generated by  $\mu$  and  $\delta$  is shown in Fig. 9. Figure 9(a) shows the SOMs colored by  $\mu$  and  $\delta$  themselves, which are the straightforward coloration patterns. The coloration pattern for  $\mu$  is from upper to bottom and the upper region has high value of  $\mu$  and the bottom region has low value of  $\mu$ . On the other hand, the coloration pattern for  $\delta$  is from left to right. The left region has high value of  $\delta$  and the right region has low value

of  $\delta$ . Figures 9(b) to (o) show the SOMs colored by  $C_L$ ,  $C_D$ , and  $C_{M_p}$  for each  $\alpha$  from  $-6$  [deg] to  $20$  [deg] with  $2$  [deg] interval. The influence of the combination between  $\mu$  and  $\delta$  on each design requirement will be observed step by step. Note that the results of the latest calibration experiment of the wind tunnel balance show to ensure the sufficient accuracy of  $C_D$  for the narrow range of  $C_D$  in Fig. 9. Therefore, discussion which Fig. 9 is employed can be implemented because Fig. 9 has the significant difference of the design requirements.

### 5.2.1 Effectiveness on $C_L$

In the first place, influence on  $C_L$  will be observed. The effectiveness of the design parameters on  $C_L$  is roughly clustered for three  $\alpha$  regions as  $\alpha \leq 0$ ,  $2 \leq \alpha \leq 12$ , and  $\alpha \geq 14$  [deg].

In the case of  $\alpha \leq 0$  [deg], specific combinations of  $\mu$  and  $\delta$  give effects on  $C_L$ . The combinations of  $\mu \geq 140$  [mm] and  $\delta \geq 8$  [deg], and the  $\mu \leq 90$  [mm] and  $\delta \leq 0$  [deg] give the effect on increasing  $C_L$ . Effectiveness on  $C_L$  is stronger as  $\alpha$  is greater in the case of the former combination. On the other hand, the combinations of  $\mu \geq 150$  [mm] and  $\delta \leq -8$  [deg], and  $\mu \leq 40$  [mm] and  $\delta \geq 6$  [deg] give the adverse effect on decreasing  $C_L$ . The magnitude of the latter adverse effectiveness is stronger than that of the former one. The adverse effectiveness on  $C_L$  is weaker as  $\alpha$  increases in the former case. That is, the effectiveness on the increase of  $C_L$  in the case of high  $\mu$  is stronger as  $\alpha$  increases. Since the separation near the tip of the main wing is restrained when the vertical control device is in the vicinity of there,  $C_L$  increases. In addition, the main wing generates the positive  $C_L$  at greater than  $\alpha_{C_{L_0}}$ . The clean configuration does not have this effectiveness. On the other hand, the latter adverse effectiveness is independent on  $\alpha$ . When the vertical control device with  $+\delta$  installs in the vicinity of the fuselage, the fuselage and the



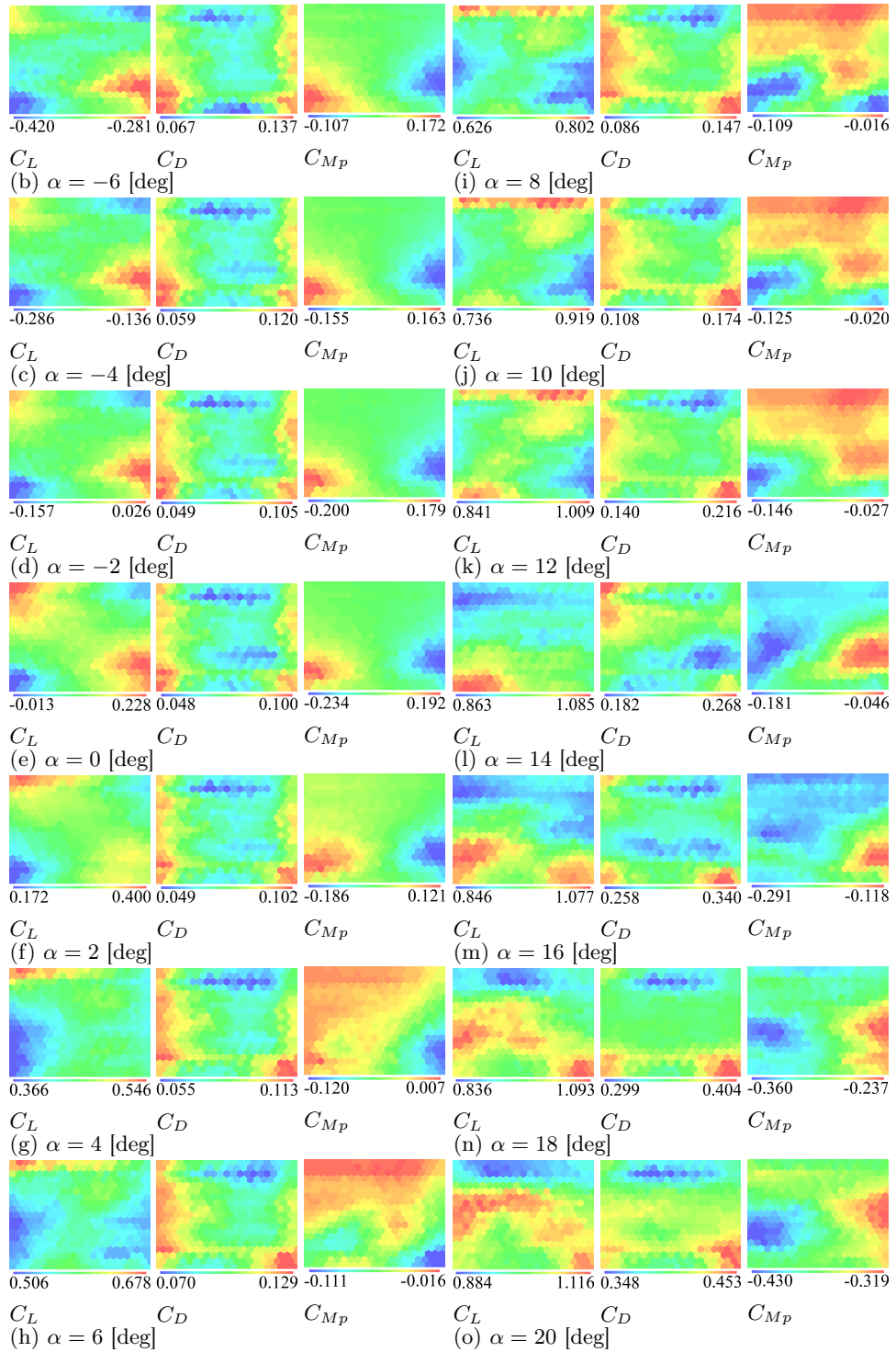


Figure 9: SOMs, (a) colored by each value of the two design parameters as  $\mu$  and  $\delta$ , (b) to (o) colored by the design requirements at each  $\alpha$ .

device generate quasi-throat flow. Since it is difficult to flow on the main-wing region where the fuselage and the device sandwich, this region is not functioning as a wing. Therefore,  $C_L$  is reduced as much.

In the case of  $2 \leq \alpha \leq 12$  [deg], the combinations between  $\mu \geq 160$  [mm] and  $\delta \geq 0$  [deg] at  $2 \leq \alpha \leq 6$  [deg], and between  $\mu \geq 160$  [mm] and all  $\delta$  at  $\alpha \geq 8$  [deg] give the effect on increasing  $C_L$ . When the vertical control device installs near the wing tip, the device functions as winglet. Therefore,  $C_L$  increases under the condition. The effectiveness under the condition that the vertical control device is near the tip disappears in the case of over  $\alpha$  of 14 [deg] because of the stall. The combination between  $\mu \leq 100$  [mm] and  $\delta \geq 6$  [deg] affects on decreasing  $C_L$ . This effectiveness is weaker as  $\alpha$  increases. The combination between  $\mu \leq 90$  [mm] and  $\delta \leq -2$  [deg] also affects on decreasing  $C_L$ . This effectiveness is stronger as  $\alpha$  increases. When the vertical control device installs around the middle of the wing, the device discourages the wing function. Since the wetted area of the vertical control device for the uniform flow is especially larger as  $|\delta|$  becomes larger, the adverse effectiveness on  $C_L$  is strong.

In the case of  $\alpha \geq 14$  [deg],  $\mu \geq 140$  [mm] affects on decreasing  $C_L$ . Especially,  $\delta \geq 0$  [deg] at  $\alpha$  of 14 [deg],  $\delta \geq 0$  [deg] and  $\delta \leq -6$  [deg] at  $\alpha$  of 16 [deg], and  $\delta$  of roughly 0 [deg] at  $\alpha$  of 18 and 20 [deg] have this effectiveness. Since the vertical control device with  $+\delta$  in the vicinity of the wing tip amplifies the tip stall,  $C_L$  sharply decreases. On the other hand, the combination between  $\mu \leq 40$  [mm] and  $\delta \geq 4$  [deg] gives the effect on increasing  $C_L$ . The upper limit of  $\mu$  to increase  $C_L$  grows as  $\alpha$  increases. In addition, the combinations between  $\mu \leq 70$  [mm] and  $\delta \geq 0$  [deg] at  $\alpha$  of 16 [deg], between  $30 \leq \mu \leq 110$  [mm] and  $\delta \geq -2$  [deg] at  $\alpha$  of 18 [deg], and between  $50 \leq \mu \leq 130$  [mm] and  $\delta \geq -4$  [deg] also give the effect on increasing  $C_L$ . Since the vertical control device at the middle of the wing exists the inside of separation due to the stall, the device reduces the pressure of its wake. As a result,  $C_L$  increases. The combination between  $\mu \leq 50$  [mm] and  $\delta \leq -2$  [deg] at  $\alpha \geq 16$  [deg] gives the effect on increasing  $C_L$ . Since the vertical control device with  $-\delta$  maintains the wing tip vortex,  $C_L$  increases.  $C_L$  is easily increased by  $\mu$  and  $\delta$  in the case of high  $\alpha$ .

### 5.2.2 Effectiveness on $C_D$

In the second place, influence on  $C_D$  will be observed. The effectiveness of the design parameters on  $C_D$  is clustered for three  $\alpha$  region as  $\alpha \leq 12$  [deg],  $\alpha$  of 14 [deg], and  $\alpha \geq 16$  [deg]. However, since  $\mu$  primarily has the effectiveness on  $C_D$ , the results will be summarized by using  $\mu$ .

$\mu$  of 150 [mm] always gives the effect on decreasing  $C_D$ . The effectiveness is not dependent on  $\alpha$ . The combination between  $\mu$  of 150 [mm] and  $-6 \leq \delta \leq 4$  [deg] especially gives more powerful effect on decreasing  $C_D$ . The magnitude of this effectiveness is similar among the cases at  $\alpha \leq 4$  [deg] and  $\alpha \geq 16$  [deg]. The magnitude of this effectiveness of  $0 < \delta \leq 4$  [deg] is stronger at  $\alpha \leq 2$  [deg]. In contrast, that of  $-6 \leq \delta \leq 0$  [deg] is stronger at  $4 \leq \alpha \leq 12$  [deg]. The magnitude of this effectiveness at  $\alpha$  of 14 [deg] is the weakest due to the existence of another combination between  $\mu$  and  $\delta$  to reduce  $C_D$  more. The separation in the vicinity of the tip of the main wing will be restrained in the case at 150 [mm]. The flow visualization of the three-dimensional space should be additionally performed in order to reveal the physical mechanism that  $\mu$  of 150 [mm] has the effectiveness on reducing  $C_D$ .

$\mu \leq 20$  and 70 [mm] also give the effect on decreasing  $C_D$ . The effectiveness does not depend on  $\alpha$ . The separation which occurs due to the interference with the fuselage will be restrained in the case at  $\mu \leq 20$  [mm] position. On the other hand, the wake of the vertical control device interferes in the tip of the horizontal tail wing in the case at  $\mu$  of 70 [mm] position. Both of these cases should not have a large  $|\delta|$  because of the larger wetted area of the vertical control device for the uniform flow.

In contrast,  $\mu$  of 40 [mm] affects on increasing  $C_D$ . The influence does not depend on  $\alpha$ . Since the wake of the vertical control device interferes the horizontal tail wing, the  $C_D$  of it increases. The flow visualization of the wake of the device should be implemented. In addition,  $C_D$  of each component should be elucidated by using computational fluid dynamics analysis.

$\delta \geq 8$  [deg] and  $\delta \leq -8$  [deg] affects on increasing  $C_D$  although  $\mu$  of 70 and 150 [mm] restricts the influence because the wetted area of the vertical control device for the uniform flow becomes large. Thereupon, a large number of  $|\delta|$  such as  $\delta \geq 8$  [deg] and  $\delta \leq -8$  [deg] should not be set in order to reduce  $C_D$ .

The case of  $\alpha$  of 14 [deg] has unique effectiveness on  $C_D$ . The combination between  $\mu$  around 60 [mm] and  $\delta$  of  $-4$  [deg] gives the effect on decreasing  $C_D$ . Since the wake of the vertical control device interferes the tip of the horizontal tail wing, the flow around the horizontal tail wing will be changed. On the other hand, the combination between  $\mu$  of 10 [mm] and  $\delta \geq 8$  [deg] and  $\delta \leq -6$  [deg] affects on increasing  $C_D$  in the case of  $\alpha \geq 16$  [deg]. The wing tip vortex is broke down because the vertical control device interferes it. The circumstantial physical mechanism to give the influence on  $C_D$  should be elucidated by using the flow visualization.

### 5.2.3 Effectiveness on $C_{Mp}$

In the third place, influence on  $C_{Mp}$  will be observed. The effectiveness of the design parameters on  $C_{Mp}$  is clustered for three  $\alpha$  regions as  $\alpha \leq 2$ ,  $4 \leq \alpha \leq 12$ , and  $\alpha \geq 14$  [deg], whose clustering is similar to that for  $C_L$ . The influence on  $C_{Mp}$  is easily understood because it depends on  $\alpha$ .

In the case of  $\alpha \leq 2$  [deg], the combination between  $\mu$  around 50 [mm] and  $\delta \geq 4$  [deg] affects on increasing  $C_{Mp}$ . On the other hand, the combination between  $\mu$  around 60 [mm] and  $\delta \leq -8$  [deg] affects on decreasing  $C_{Mp}$ . This change of  $C_{Mp}$  is explained by the function on the main-wing region where the fuselage and the vertical control device sandwich, that is similar mechanism of  $C_L$ .

In the case of  $4 \leq \alpha \leq 12$  [deg], the effectiveness is clustered by using  $\mu$ . The case of  $\mu \geq 150$  [mm] affects on increasing  $C_{Mp}$ . It is independent of  $\delta$ . Since this area on SOM has large  $C_L$  and small  $C_D$ ,  $C_{Mp}$  naturally increases. The combination between  $\mu$  around 50 [mm] and  $\delta \geq 4$  [deg] affects on decreasing  $C_{Mp}$ . The result is occurred by the similar mechanism in the above case of  $\alpha \leq 2$  [deg]. The combination between  $\mu \leq 90$  [mm] and  $\delta \leq -4$  [deg] also affects on decreasing  $C_{Mp}$ . Since the wake of the vertical control device interferes the tip of the horizontal tail wing, the tip vortex of the horizontal tail wing is induced. Therefore, the total  $C_{Mp}$  is reduced.

In the case of  $\alpha \geq 14$  [deg], the combination between  $50 \leq \mu \leq 80$  [mm] and  $\delta \leq -4$  [deg] affects on increasing  $C_{Mp}$ . This is caused by the interference of the wake of the device with the tip of the horizontal tail wing. On the other hand, the combination between  $40 \leq \mu \leq 70$  [mm] and  $\delta \geq 4$  [deg] affects on decreasing  $C_{Mp}$ . The result is occurred by the similar mechanism in the above case of  $\alpha \leq 2$  [deg]. Moreover,  $\mu \geq 140$  [mm] also affects on decreasing  $C_{Mp}$  except for the case of  $\alpha$  of 20 [deg]. This does not depend on  $\delta$ . The result is induced by decreasing  $C_L$ .

$C_{Mp}$  directly depends on  $C_L$ ,  $C_D$ , and  $\alpha$ . In addition, the trim of the aircraft is practically gained to control elevators. Thereupon, it is considerable that the design knowledge regarding  $C_L$  and  $C_D$  is primary and the design knowledge regarding  $C_{Mp}$  is secondary.

## 6 Conclusions

The new concept to place the vertical airfoil device as control surface has arrived in so as to improve the aerodynamic performance. The wind tunnel experiment has been implemented in order to investigate the influence of the vertical control device with symmetrical airfoil shape. Moreover, data min-

ing has been performed by using a self-organizing map for the experimental data in order to qualitatively reveal the correlations among the aerodynamic performances and the design parameters to place the vertical control device. Consequently, it has been revealed the correlations among them. Furthermore, there is a sweet spot, where is at  $\mu$  around 150 [mm] and  $-4 \leq \delta \leq 4$  [deg], in the present design space. In addition, the especial design parameters to improve the aerodynamic performance have been specified by using the data mining so that the detailed flow condition is observed. The three-dimensional geometry of vertical control device in the sweet spot will be optimized as the subsequent design phase based on the extracted design knowledge.

## Acknowledgment

The present study was supported by Japan Society for the Promotion of Science through a Grant-in-Aid for Challenging Exploratory Research 26630440.

## References

- [1] K. Chiba and S. Obayashi. Knowledge discovery in aerodynamic design space for flyback-booster wing using data mining. *Journal of Spacecraft and Rockets*, 45(5):975–987, 2008.
- [2] G. Deboeck and T. Kohonen. *Visual Explorations in Finance with Self-Organizing Maps*. London, Springer Finance, 1998.
- [3] M. Fujino. Design and development of HondaJet. *Journal of Aircraft*, 42(3):755–764, 2005.
- [4] M. Fujino and Y. Kawamura. Wave-drag characteristics of an over-the-wing nacelle business-jet configuration. *Journal of Aircraft*, 40(6):1177–1184, 2003.
- [5] T. Kohonen. *Self-Organizing Maps*. Springer, Berlin, Heidelberg, 1995.
- [6] J. C. Lin. Review of research on low-profile vortex generators to control boundary-layer separation. *Progress in Aerospace Sciences*, 38(4):389–420, 2002.

- [7] T. Omori, Y. Sunada, and T. Imamura. Experimental and numerical research on aerodynamic characteristics of rectangular fin mounted vertically over the wing. AIAA Paper 2015-0774, 2015, 2015.
- [8] O. Samoylovitch and D. Strelets. Determination of the Oswald efficiency factor at the aeroplane design preliminary stage. *Aircraft Design*, 3(3):167–174, 2000.
- [9] D. A. Solfelt and R. C. Maple. CFD analysis of a T-38 wing fence. AIAA Paper 2008-0331, 2005.